



Quantitative examination of an unconventional form of the filled-space illusion

Aleksandr Bulatov^{1,2} · Natalija Bulatova² · Edgaras Diržius²

Accepted: 19 March 2021 / Published online: 31 March 2021
© The Psychonomic Society, Inc. 2021

Abstract

The spatial interval containing some visual elements (fillers) seems to be longer than an empty interval of the same length, and the effect persists for most observers. This illusion of interrupted spatial extent (or the filled-space illusion) can be observed even in extremely simplified line drawings, but its origin is still not completely understood. Recently, we proposed a quantitative explanation for the results of experiments with stimuli containing either continuous or discrete filling: the illusion may be associated with the integration of distractor-induced effects near the endpoints (terminators) of the stimulus intervals. Subsequent analysis of the principles underlying the explanation allowed us to hypothesize the appearance of illusory effects caused by previously unknown stimulus modifications. To test the suggestions, in the present study we performed experiments with three-dot stimuli that contain a distracting circle (either outline or uniformly filled) surrounding one of the lateral terminators. It has been demonstrated that the illusion magnitude varies predictably with the size of the circle, and there is no significant difference between the data obtained for stimuli with the outline and filled distractors. To more thoroughly examine the illusion, the central angle of circular distracting arcs (real or imaginary) was used as an independent variable in supplementary experiments. A rather successful theoretical interpretation of the experimental results supports the suggestion that perceptual positional biases induced by additional context-evoked neural excitation can be considered as one of the main causes of the filled-space illusion.

Keywords Length misjudgment · Filled-space illusion · Weighting profile of spatial summation · Oppel-Kundt illusion

Introduction

It is well known that more or less discernible inconsistency between the perceived object's properties and what exists in the external world accompanies the activity of all sensory modalities. Classic examples of this phenomenon are the so-called geometric-optical illusions, in particular, the illusions of extent (or length) that arise when comparing the linear dimensions of different parts of the image. These illusions have long been studied because their occurrence indicates not only some failures in perception, but also helps to reveal organization of underlying neural mechanisms adapted for optimal

performance of appropriate range of visual tasks (Morgan et al., 1990), thereby contributing to a better understanding of the general principles of visual perception of spatial relationships.

One of the most famous representatives of geometric-optical illusions, the so-called Oppel-Kundt illusion (or the filled-space illusion, FSI), occurs when viewing extremely simple flat drawings (Fig. 1): a spatial interval containing some distracting visual elements (fillers) appears to be larger than an empty interval of the same length, and the effect is remarkably robust for most observers. Throughout a rather long history of research, the illusion was tested changing various parameters of a number of stimulus modifications: the amount or density of discrete fillers (Bertulis & Bulatov, 2001; Bulatov et al., 1997; Coren et al., 1976; Noguchi, 2003; Noguchi et al., 1990; Obonai, 1933; Piaget & Osterrieth, 1953; Spiegel, 1937; Wackermann & Kastner, 2009; Wackermann & Kastner, 2010); the spatial frequency of filling the textured area (Giora & Gori, 2010); luminance or color contrast between stimulus elements (Bulatov & Bertulis, 2005; Long & Murtagh, 1984; Surkys, 2007; Wackermann,

✉ Aleksandr Bulatov
aleksandr.bulatov@ismuni.lt

¹ Laboratory of Visual Neurophysiology, Lithuanian University of Health Sciences, Mickevičiaus 9, LT-44307 Kaunas, Lithuania

² Institute of Biological Systems and Genetics Research, Lithuanian University of Health Sciences, Mickevičiaus 9, LT-44307 Kaunas, Lithuania



Fig. 1 Examples of stimuli that induce the filled-space illusion. The conventional Oppel-Kundt figure with equally spaced distracting fillers (**upper**), and the three-dot figure with continuous filling by a line-segment (**lower**)

2012); the temporal duration of stimulus presentation (Bailes, 1995; Bertulis et al., 2014; Dworkin & Bross, 1998). At the same time, despite the seeming simplicity of the phenomenon, the current understanding concerning the origin of the FSI (and related illusions) is still far from complete (cf. Wackermann, 2017), and the known (rather few) explanations are mainly qualitative (i.e., not supported by the relevant quantitative analysis). For example, the Oppel-Kundt illusion may be related to the perception of a well-defined spatial separation of contextual fillers (Taylor, 1962) and is presumably determined by the number of zero-crossings in the spatial profile of the corresponding neural excitation (Craven & Watt, 1989; Watt, 1990). According to other theoretical approaches, the emergence of the illusion may be associated with neural processes of lateral inhibition (Blakemore et al., 1970; Ganz, 1966) or bandpass spatial frequency filtering (Bulatov et al., 1997; Surkys, 2007), which can lead to perceptual repulsion of stimulus elements.

Recently, it was demonstrated (Bulatov et al., 2017) that the FSI can be associated mainly with effects caused by contextual distractors in the close surrounding of the terminators of stimulus spatial intervals. Subsequent studies (Bulatov et al., 2019) made it possible to propose a rather simple quantitative explanation for the FSI, based on the idea that length misjudgments arise due to the local integration of context-induced additional excitation during visual assessment of objects' retinal coordinates. In the FSI model, it was assumed that the coordinates are encoded by the magnitude of the cumulative neural response of some hypothetical area of weighted spatial integration (AWS) centered on the object, and that the size of the AWS increases linearly with its retinal eccentricity. Since the greater eccentricity is also associated with a wider aggregated profile of the neuronal population receptive field (Dekker et al., 2019; Dumoulin & Wandell, 2008; Silva et al., 2018; Welbourne et al., 2018), a larger response of the relevant AWS can be expected, thus providing mutual correspondence between the magnitude of neural activity and the perceived location of the object. Accordingly, for the FSI, the presence of contextual distractor near the stimulus terminator increases the cumulative response of the AWS centered at the terminator, and this increase in response is decoded by the visual system as a displacement in the perceived location of the terminator.

The supposition is consistent with the results of extracellular recordings (Bremmer et al., 2016; Graf & Andersen, 2014; Sereno & Lehky, 2011; Steenrod et al., 2013), which demonstrated that changes in the magnitude of neuronal responses in the macaque lateral intraparietal cortex reliably provide information about the target's location as well as the size of the upcoming saccade. In turn, to ensure amplitude-independent conditions for unambiguous coding of the coordinates, an additional important assumption was made in the FSI explanation regarding scaling (or normalization) to a certain constant range of AWS input neural activity, and this assumption is also in agreement with numerous literature data (Carandini & Heeger, 2012; Olsen et al., 2010; Reynolds & Heeger, 2009; Vokoun et al., 2014).

The proposed explanation of the FSI provided a rather successful interpretation of experimental results with various modifications of stimuli comprising either discrete or continuous filling (Bulatov et al., 2017; Bulatov et al., 2019; Marma et al., 2020), which also demonstrated that the illusion manifests similarly for a single distractor located either inside or outside the stimulus interval, and that the illusory effects are about twice as strong in the case of two distractors located symmetrically with respect to the lateral terminator. We think that this significant enhancement of illusory effects can be considered as a specific feature that distinguishes the FSI from the Müller-Lyer illusion, which practically disappears due to opposite signs of the effects caused by symmetrically arranged distractors.

Subsequent more thorough analysis of the basic computational principles underlying the FSI explanation allowed to suggest the appearance of illusory effects caused by previously unknown stimuli containing contextual distracting circles or circular arcs (Fig. 2). Therefore, if the illusion actually arises, the main goal of the present study was to further develop the model by testing its applicability for quantitative prediction of the results of psychophysical experiments with these new illusory patterns, which, at first glance, are completely different from conventional stimuli such as, for example, the Oppel-Kundt figures or those with continuously filled spatial intervals (Fig. 1). We think that such a quantitative computational approach in the illusions research provides a rather interesting and potentially fruitful way for further investigations, as it allows immediate and targeted

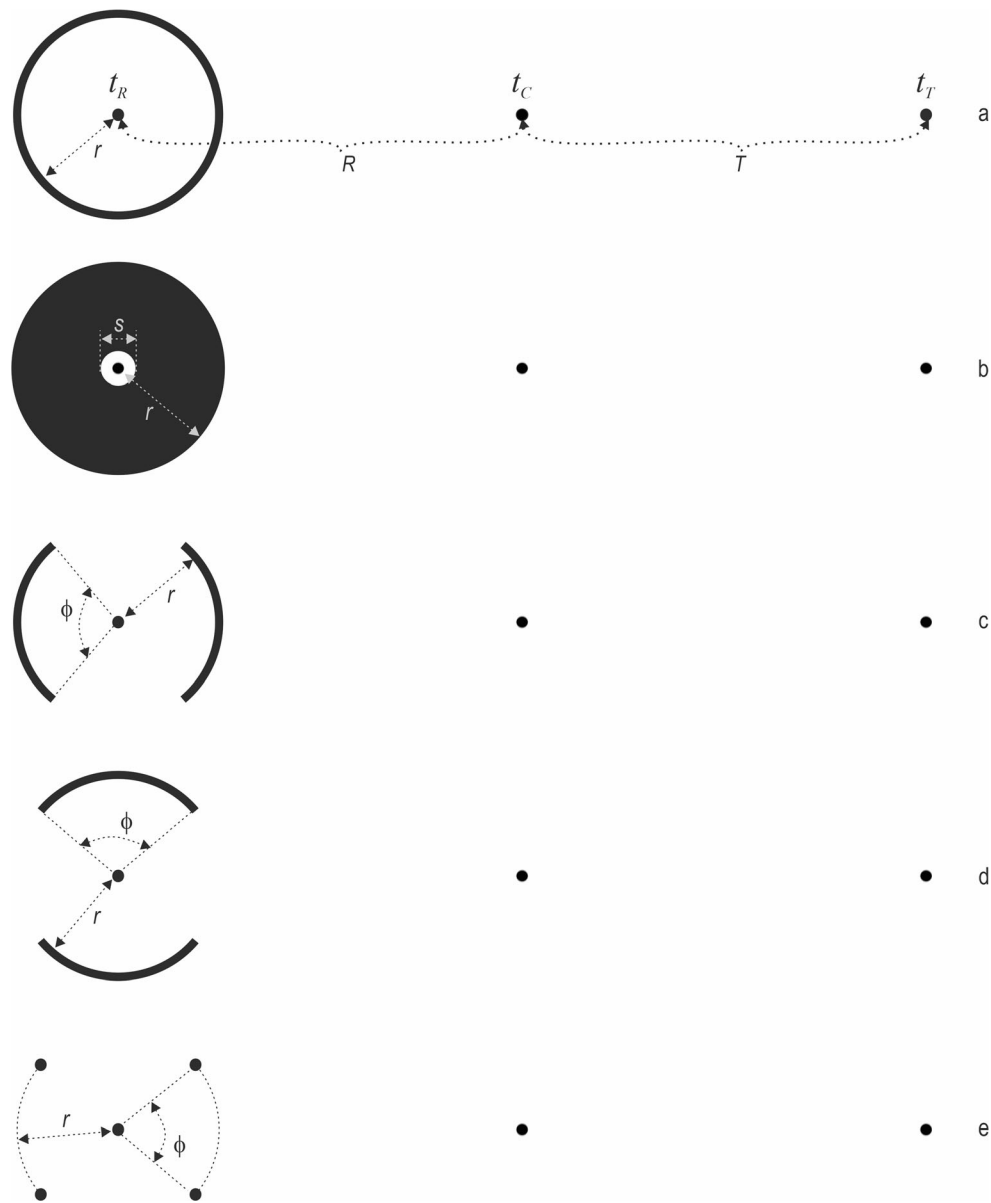


Fig. 2 Examples of different types of contextual distractors used in the study. The three-dot (t_R , t_C , and t_T) stimuli with various distractors arranged symmetrically with respect to the lateral terminator (t_R): the outlined circle (a), the uniformly filled circle (b), the circular arcs oriented orthogonally (c) and parallel (d) to the main stimulus axis, and the endpoints of imaginary arcs (e). R and T the length of the reference and test

interval, respectively; r the radius of the circle; s the diameter of the unfilled area; ϕ the central angle of the arcs. In experiments, white stimuli (luminance of all the dots and lines, 20 cd/m^2) were presented against a dark round-shaped background (8° in diameter and 0.4 cd/m^2 in luminance)

experimental verification (with possible refutation) of theoretical assumptions.

Theoretical predictions

Here, we briefly introduce the model's computational procedures used in the study. It was shown (Bulatov et al., 2020) that the two-dimensional profile of the AWS can be described as the product of two functions: the absolute value of the first derivative of a Gaussian along the main stimulus x -axis (i.e.,

along which the length judgments are performed) and the Gaussian function along the orthogonal y -axis (Fig. 3a):

$$\begin{aligned}
 W(x, y, \sigma) &= \left(\frac{|x|}{\sigma^2} e^{-\frac{x^2}{2\sigma^2}} \right) e^{-\frac{y^2}{2\sigma^2}} \\
 &= \frac{|x|}{\sigma^2} e^{-\frac{x^2+y^2}{2\sigma^2}}, \text{ or in polar coordinates, } W(\rho, \phi, \sigma) \\
 &= \frac{|\rho \cos(\phi)|}{\sigma^2} e^{-\frac{\rho^2}{2\sigma^2}}
 \end{aligned} \tag{1}$$

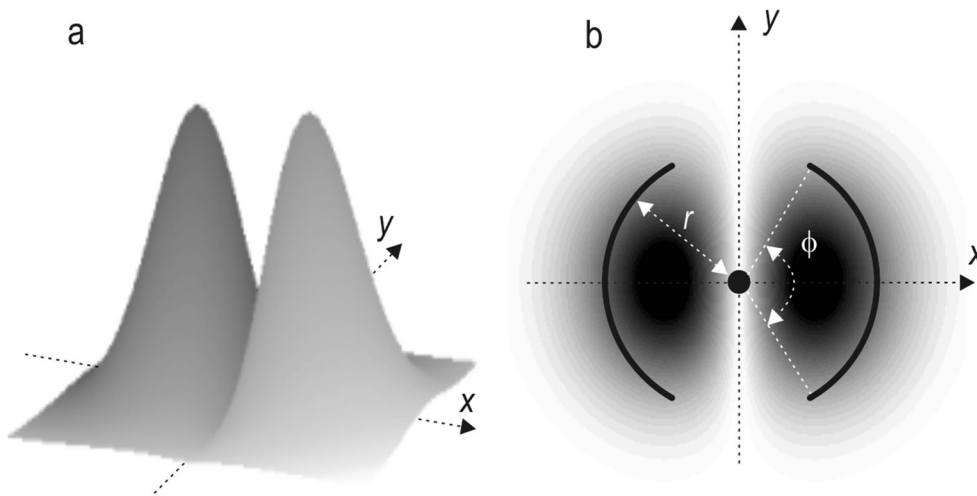


Fig. 3 Diagrams illustrating the calculations. **a** Two-dimensional view of the weighting profile, $W(x,y,\sigma)$, of the AWS represented by the absolute value of the first derivative of Gaussian and the Gaussian functions in mutually orthogonal stimulus axes x and y . **b** Diagram illustrating the

calculations according to formula 2 (for illustrative purposes, only the two-dimensional profile of the AWS, centered at the stimulus terminator-dot, is shown as the gray-level intensity distribution)

where σ represents the standard deviation.

Given the model’s assumption that the illusion occurs due to the distractor-induced additional neural excitation, in the case of two vertical circular arcs (arranged symmetrically with respect to the stimulus terminator, Fig. 3b), the illusion

magnitude can be estimated by weighted integration over the positive part of the function, which is the difference between the two-dimensional profiles of stimulus-evoked excitation with and without distractors:

$$A_{ver}(r, \phi, \sigma, k) \approx k \int_0^{\frac{\phi}{2}} \left(\int_{-\frac{r}{\sigma}}^{\frac{r}{\sigma}} W(\rho, \alpha, \sigma) (D_{out}(\rho, r, \sigma) - T(\rho, \sigma)) \rho d\rho \right) d\alpha = k \int_0^{\frac{\phi}{2}} \cos(\alpha) \left(\int_{-\frac{r}{\sigma}}^{\frac{r}{\sigma}} \frac{\rho^2}{\sigma^2} \left(e^{-\frac{\rho^2 + (r-\rho)^2}{2\sigma^2}} - e^{-\frac{\rho^2}{\sigma^2}} \right) d\rho \right) d\alpha = \frac{k}{4} \sin\left(\frac{\phi}{2}\right) \left(\left(\frac{(r^2 + 2\sigma^2)\sqrt{\pi}}{2\sigma} + r \right) e^{-\frac{r^2}{4\sigma^2}} + \sigma\sqrt{\pi} \left(\operatorname{erf}\left(\frac{r}{2\sigma}\right) - 1 \right) \right) = \sin\left(\frac{\phi}{2}\right) C_{out}(r, \sigma, k) \tag{2}$$

where k is some coefficient of proportionality; r and ϕ represent the radius and central angle of the arc, respectively; $T(\rho, \sigma) = e^{-\frac{\rho^2}{2\sigma^2}}$ and $D_{out}(\rho, r, \sigma) = e^{-\frac{(\rho-r)^2}{2\sigma^2}}$ represent the normalized radial profiles of neural excitation evoked by the terminator-dot and the arc, respectively (for simplicity, the same standard deviation, σ was assumed for Gaussian profiles of neural excitation and AWS); $C_{out}(r, \sigma, k)$ is the illusion magnitude caused by a full outlined circle (Fig. 2a). In turn, for horizontal distracting arcs (Fig. 2d), formula 2 needs to be

modified as follows:

$$A_{hor}(r, \phi, \sigma, k) \approx \left(1 - \cos\left(\frac{\phi}{2}\right) \right) C_{out}(r, \sigma, k) \tag{3}$$

In a similar way, the dependence of the illusion magnitude on the radius of the uniformly filled circle (Fig. 2b) can be evaluated by the formula:

$$C_{fld}(r, \sigma, k) \approx k \int_0^{\frac{\pi}{2}} \left(\int_{-\frac{r}{\sigma}}^{\frac{r}{\sigma}} W(\rho, \alpha, \sigma) (D_{fld}(\rho, r, \sigma) - T(\rho, \sigma)) \rho d\rho \right) d\alpha \approx k \int_0^{\frac{\pi}{2}} \cos(\alpha) \left(\int_{-\frac{r}{\sigma}}^{\frac{r}{\sigma}} \frac{\rho^2}{\sigma^2} e^{-\frac{\rho^2}{2\sigma^2}} \left(\left[H\left(\rho - \frac{s}{2}\right) - H(\rho - r) \right] - e^{-\frac{\rho^2}{2\sigma^2}} \right) d\rho \right) d\alpha = \frac{k}{4} \left(\sqrt{\pi}\sigma \left(\operatorname{erf}\left(\frac{s}{2\sigma}\right) - \operatorname{erf}\left(\frac{r}{\sigma}\right) \right) + 2\sqrt{2} \left(\operatorname{erf}\left(\frac{r}{\sqrt{2}\sigma}\right) - \operatorname{erf}\left(\frac{s}{2\sqrt{2}\sigma}\right) \right) \right) + 2re^{-\frac{r^2}{2\sigma^2}} \left(e^{-\frac{r^2}{2\sigma^2}} - 2 \right) - se^{-\frac{s^2}{8\sigma^2}} \left(e^{-\frac{s^2}{8\sigma^2}} - 2 \right) \tag{4}$$

where s is the diameter of the unfilled central area. Here, for simplicity (bearing in mind the effect of strong attenuation

towards the periphery of the Gaussian profile of the AWS), the radial profile of the distractor-evoked excitation was

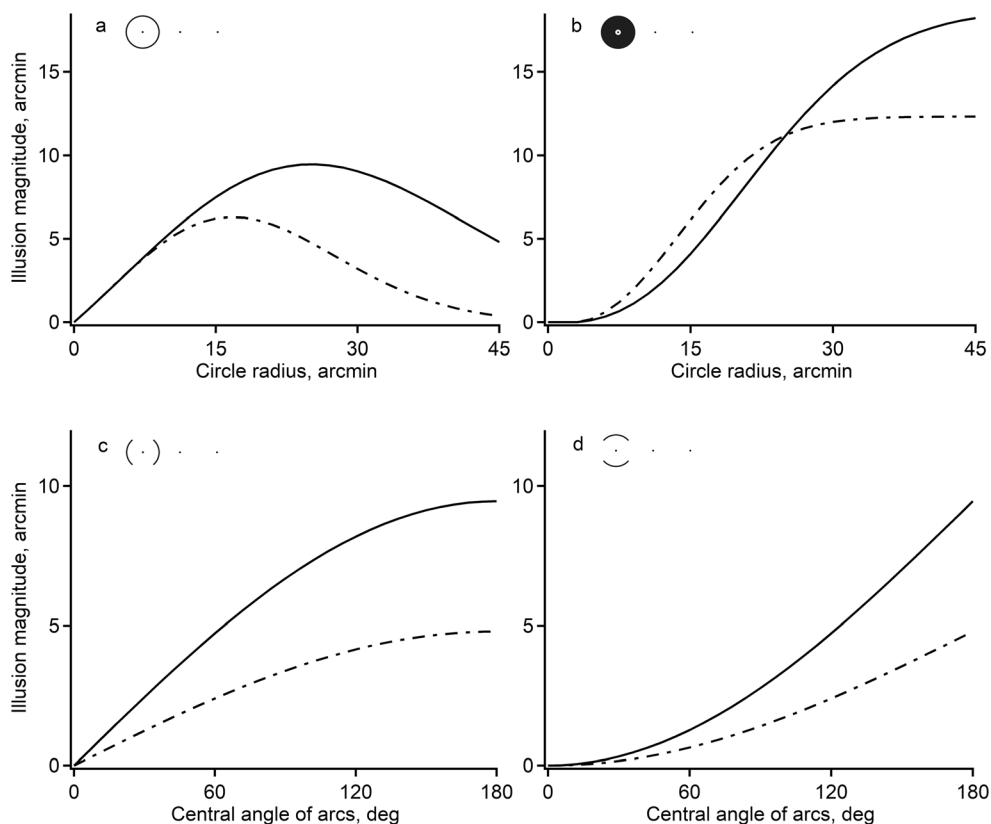


Fig. 4 The model predictions of the illusion magnitude. In the graphs, solid and dash-dot curves represent data for stimuli with the outlined circle (a), the uniformly filled circle (b), the vertical arcs (c), and the horizontal arcs (d), respectively. In calculations, the coefficient k was

always equal to 1, and parameter σ , which specify the size of the AWS, was equal to 10 (dash-dot curves) or 15 (solid curves) arcmin; the arc's radius r was equal to 25 arcmin

approximated by a piecewise-constant function not convolved with a Gaussian kernel (i.e., the difference of two Heaviside step functions H was used instead of the rather complex function D_{fd}).

As can be seen from the graphs in Fig. 4, the model calculations predict a rather simple shape of curves of the illusion dependence on the size of distracting circle surrounding the lateral stimulus terminator. The illusion magnitude increases with increasing to a certain value of the radius of the distractor and then gradually decreases in the case of an outlined circle (Fig. 4a), but remains at the constant level for the uniformly filled circle (Fig. 4b). In both cases, the illusion magnitude considerably depends on the size of the relevant AWS (different values of the standard deviation, σ); it should also be noted that the calculated maximum illusion values for filled distractors are significantly larger than those for the outlined circles. Regarding stimuli with two circular arcs arranged symmetrically relative to the lateral terminator, the model predicts the dependence of the illusion magnitude on the arc angle, ϕ as proportional to $\sin(\phi/2)$ and $1-\cos(\phi/2)$, for vertically (Fig. 4c) and horizontally (Fig. 4d) oriented arcs, respectively.

Obviously, formulas 2–4 provide an extremely simplified assessment of the FSI behavior, since a number of potentially

important concomitant factors were not considered in the modeling. For instance, the present model calculations did not concern the effects of spatial differentiation caused by spatial-frequency filtering. These effects can be practically indiscernible in the case of simple continuous stimuli, such as full outlined circles, because they do not essentially distort the spatial structure of the corresponding profiles of neural excitation. At the same time, the manifestation of spatial differentiation effects can be significant for stimuli with a number of abrupt changes (such as surface boundaries or endpoints of lines) in the luminance profile. For example, calculations using formula 2 predict the disappearance of the illusion for very short vertical arcs (i.e., for dots); however, our previous study of the FSI (Bulatov et al., 2019) demonstrated a rather strong illusion caused by separate distracting dots located on the main stimulus axis. Thus, a quantitative theoretical description of experimental results for such discontinuous stimuli may require certain additional modifications in the model calculations; however, the analytical implementation of these modifications can be associated with significant computational difficulties.

Since the illusion magnitude may strongly depend on the size of relevant AWS (thereby, on its retinal eccentricity that varies with the actual direction of gaze), the curves in Fig. 4

should be considered only as illustrating some idealized static conditions of stimuli observation. However, we expected that it would be possible to establish a certain agreement between the model predictions and the averaged experimental results.

Methods

Apparatus

All experiments were carried out in a dark room (the surrounding illumination $< 0.2 \text{ cd/m}^2$). A Sony SDM-HS95P 19-in. LCD monitor (spatial resolution $1,280 \times 1,024$ pixels, frame refresh rate 60 Hz) was used for the stimuli presentations. A Cambridge Research Systems OptiCAL photometer was applied to the monitor luminance range calibration and gamma correction. A chin and forehead rest was used to maintain a constant viewing distance of 200 cm (at this distance each pixel subtended about 0.5 arcmin); an artificial pupil (an aperture with a 3-mm diameter of a diaphragm placed in front of the eye) was applied to reduce optical aberrations.

Stimuli were presented in the center of a round-shaped background of about 8° in diameter and 0.4 cd/m^2 in luminance (the monitor screen was covered with a black mask with a circular aperture to prevent observers from being able to use the edges of the monitor as a vertical/horizontal reference). For all the stimuli drawings, the Microsoft GDI+ antialiasing technique was applied to avoid jagged-edge effects.

Stimuli

The stimuli used in the study comprised three base dots (dot-size, 3 arcmin; luminance, 20 cd/m^2) arranged horizontally, which were considered as terminators (t_R , t_C , and t_T , Fig. 2a) specifying the ends of the reference and test stimulus intervals. In all experiments, the length (R) of the reference interval was fixed at 90 arcmin and the subjects changed the length (T) of the test interval by adjusting the position of the lateral terminator (t_T) so that both intervals were perceived as equal in length.

In Experiment 1, the radius (r) of the distracting circle surrounding the lateral terminator (t_R) was used as an independent variable, which changed randomly in a range from 0 to 45 arcmin. In the first series of Experiment 1, stimuli (Fig. 2a) with outlined circles (line-width, 2 arcmin; luminance, 20 cd/m^2) were presented. In the second series of Experiment 1, uniformly filled circles (luminance, 20 cd/m^2 ; the diameter, s of the central unfilled area, 8 arcmin) were used (Fig. 2b).

In Experiment 2, the two distracting circular arcs (line-width, 2 arcmin; luminance, 20 cd/m^2 ; circle radius, 25 arcmin) were arranged symmetrically with respect to the lateral stimulus terminator (t_R) and the central angle (ϕ) of the

arcs was used as an independent variable, which randomly changed in a range from 0° to 180° . In the first series of Experiment 2, stimuli (Fig. 2c) with vertical circular arcs (i.e., oriented orthogonally to the main stimulus axis) were presented. In the second series, horizontally oriented arcs were used as contextual distracting elements (Fig. 2d).

In Experiment 3, the independent variable was the same as in the first series of Experiment 2 (i.e., the central angle of arcs, ϕ); however, only the endpoints (dot-size, 2 arcmin; luminance, 20 cd/m^2) of imaginary arcs were visible to observers (Fig. 2e).

Procedure

The method of adjustment was used in the study: during the experimental run, the subjects were asked to manipulate the keyboard buttons “←” and “→” to move the lateral terminator t_T of the test interval into a position that makes both stimulus parts perceptually equal in length (Fig. 2a). The physical difference between the lengths of the test and reference intervals, $I = T - R$, was considered as the illusion magnitude; the values of the relative overestimation of the reference interval length, $rI = \frac{I}{R} 100\%$, were also used. A single button push varied the position of the terminator by one pixel corresponding approximately to 0.5 arcmin. The initial length differences between the stimulus intervals were randomized and distributed evenly within a range of ± 10 arcmin.

The subjects were instructed to maintain their gaze on the central stimulus terminator; however, observation time was not limited, and subjects' eye movements were not registered. A combination of two types of stimulus presentation conditions (for different conditions the stimulus orientation differed by 180° , i.e., the reference and test stimulus parts were swapped) was used in each experimental run. Trials from different conditions were randomly interleaved to minimize (by averaging subjects' responses) effects of the left/right visual field anisotropy and reduce stimulus persistence. An experimental run took about half an hour and included 124 stimulus presentations, that is, 31 different values of the independent variable for each stimulus condition were taken (in a pseudo-random order) twice. For each type of stimulus, each subject carried out at least five experimental runs on different days (i.e., at least ten trials went into the analysis of each data point).

Subjects

Data were collected from seven human observers (19- to 32-year-old, five males and two females), who were naïve to the purpose of the study, and all had normal or corrected-to-normal vision. With the aim of providing more strict viewing

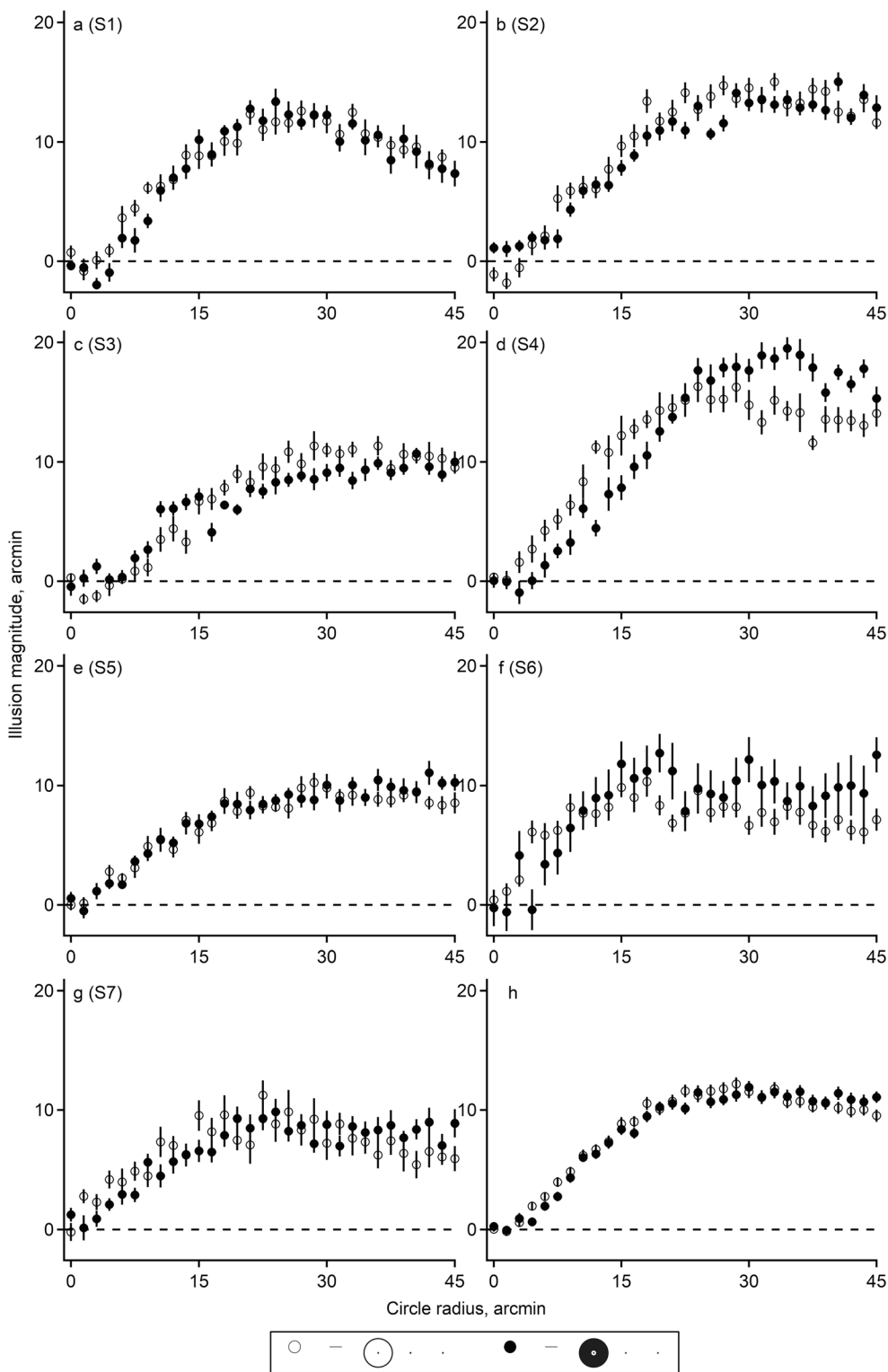


Fig. 5 The illusion magnitude as a function of the radius of distracting circles. In the graphs, *open* and *closed* symbols represent the data for stimuli with the outlined and uniformly filled distractors, respectively.

Error bars depict ± 1 standard error of the mean (SEM). Graphs (a–g) represent data for subjects S1–S7 and (h) represents the grand-mean data

conditions and eliminate potential effects related to binocularity, the right eye was always tested irrespective of whether it was the leading eye or not. All subjects gave their informed

consent before taking part in the experiments performed in accordance with the ethical standards of the Declaration of Helsinki.

Results

Experiment 1: Length misjudgments induced by distracting circles

The aim of the experiment was to verify the prediction that the presence of a distracting circle surrounding the lateral stimulus terminator could cause length-matching errors and, if so, to quantify the dependence of the illusion magnitude on the radius of the circle. In the first series of Experiment 1, stimuli with an outlined distractor (Fig. 2a) were used; the circle radius randomly varied in a range from 0 to 45 arcmin.

As can be seen from the graphs in Fig. 5a–g (open circles), despite some inter-individual difference, the experimental results from all the subjects yielded curves of a similar simple shape. The illusion magnitude smoothly increases from about zero to maximum value (on average, $rI \approx 13\%$) with an increase in the radius of the distractor to about one-third of the length of the reference interval (the position and value of the maximum vary slightly for different subjects), and then demonstrates some tendency to decrease; thus, the behavior of the illusion is in good agreement with that of the predicted outcome.

We suppose that inter-individual variability in results may be primarily due to the inherent inaccuracy of the method of adjustment, for example, errors caused by biases in judgment and decision-making (Morgan et al., 2013), as well as due to a subject-specific pattern of gaze fixations and distribution of attention during stimulus observations (Krauzlis et al., 2017). To estimate the general trend of the results for the whole group of observers, the grand-mean curve was calculated (Fig. 5h; open circles). We think that rather small values of SEM (not exceeding 0.57 arcmin) for the grand-means data indirectly support our assumption regarding the similarity of the shape of the individual curves.

In the second series of Experiment 1, stimuli with uniformly filled distracting circles (Fig. 2b) were used. To ensure clear discrimination of the stimulus terminator, a small circular area (diameter about 8 arcmin) remained unfilled in the distractor center. We think that a rather interesting and unexpected result of this series is related to the fact that experimental curves obtained for most subjects (Fig. 5a–g; closed circles) are practically identical to those gathered in experiments with outlined distractors. As well as in the first series of Experiment 1, the illusion magnitude dependence on the distractor radius can be more easily seen for the grand-mean curve calculated for the entire group of observers (Fig. 5h; closed circles); the values of SEM for the grand means do not exceed 0.61 arcmin. Comparison of the grand means for stimuli with two different types of distractors (outlined or uniformly filled) did not reveal a statistically significant difference (the paired t -test, $df = 30$, $\alpha = 0.05$: $t = 0.924$ [$P = 0.363$] with the preliminary Shapiro-Wilk test for the normality of residuals: $W = 0.981$ [$P = 0.828$]). The results of a two-way ANOVA for empirical

data from all observers (distractor type factor: $F(1,30) = 0.206$ [$P = 0.653$]; the Shapiro-Wilk test for normality: $W = 0.966$ [$P = 0.426$]) additionally confirm the similarity in the illusion behavior for outlined and uniformly filled distractors.

This absence of difference is somewhat inconsistent with our preliminary theoretical suggestion that (in the case of the same stimulus-viewing conditions) the illusion for uniformly filled circles should be considerably stronger than that for the outlined ones (Fig. 4). Therefore, we supposed that this fact may be associated with the over-simplification of our current modeling that did not take into account the processes of two-dimensional spatial frequency filtering (contour extraction due to the spatial differentiation procedure), which can substantially enhance the similarity between the excitation profiles caused by outlined and uniformly filled visual objects with the same boundary shape, thereby leading to the resemblance of experimental curves obtained from different series.

Experiment 2: Illusion caused by distracting circular arcs

For additional assessment of the illusion properties, we used stimuli with circular arcs that were arranged symmetrically with respect to the lateral stimulus terminator and oriented orthogonally (Fig. 2c) or parallel (Fig. 2d) to the main stimulus axis. The radius of arcs was fixed at 25 arcmin, and their central angle (ϕ) was used as the independent variable (randomly changed in a range from 0° to 180°). According to our simplified preliminary quantitative estimates (formulas 2 and 3), the dependence of the illusion magnitude on the arc angle should be proportional to $\sin(\phi/2)$ in the case of vertical arcs and proportional to $1 - \cos(\phi/2)$ for horizontal arcs.

As can be seen from the graphs in Fig. 6a–g (open circles), the results of the first series of Experiment 2 (vertical arcs) strongly deviate from the model predictions. For most subjects, the illusion magnitude increases sharply from approximately zero (at $\phi = 0^\circ$, i.e., when there are no distractors) to the maximum value (on average, $rI \approx 15\%$; arc angle within the range 6 – 18°), and then slowly decreases (there is a slight difference for subject S7, Fig. 6g) with increasing arc angle up to about 60° . With a further increase in the angle to 180° , the experimental curves are almost parallel to the abscissa axis (on average, $rI \approx 13\%$). As in the previous series of experiments, the grand-mean curve was calculated from the individual data of the entire group of observers (Fig. 6h; open circles); the values of SEM for the grand means do not exceed 0.66 arcmin.

The results of the second series of Experiment 2 (i.e., with circular arcs oriented horizontally) are more consistent with the predictions and gave curves showing a gradual increase in the magnitude of the illusion with an increase in the central angle of the arcs. As can be seen from the graphs in Fig. 6a–g (closed circles), for all subjects, the magnitudes of length misjudgments when the central angle approaches 180° (i.e., when

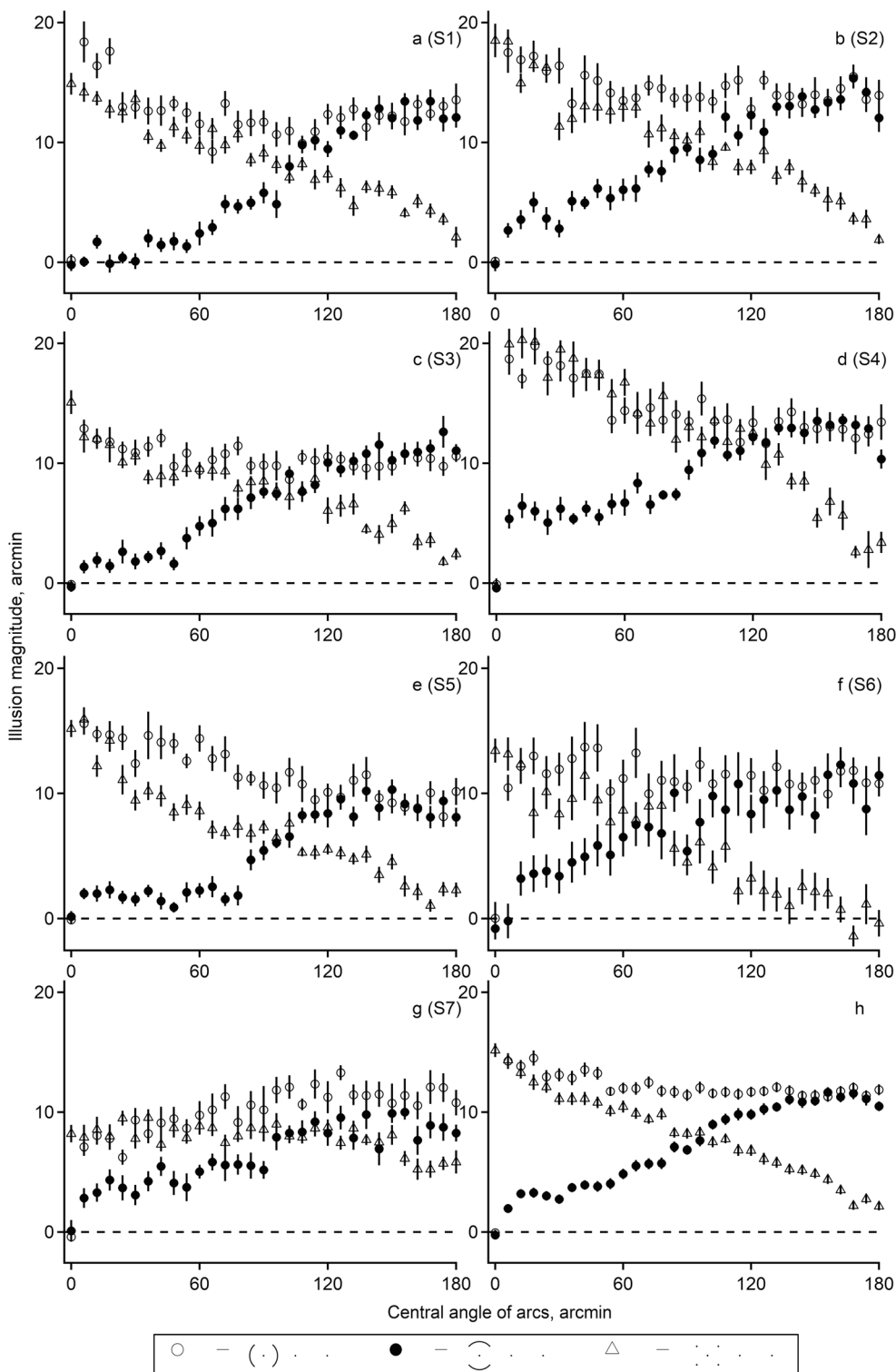


Fig. 6 The illusion magnitude as a function of the central angle of distracting circular arcs. In the graphs, open and closed circles represent the data for stimuli with the vertical and horizontal arcs, respectively;

triangles represent the data for stimuli with endpoints of imaginary arcs. Error bars depict ± 1 standard error of the mean (SEM). Graphs (a–g) represent data for subjects S1–S7 and (h) represents the grand-mean data

two distracting arcs merge into a circle) are approximately equal to the corresponding values from the previous series of Experiment 2, and are also consistent with data obtained in the first series of Experiment 1 for the distracting outlined

circle with a radius of 25 arcmin. We believe that this fact demonstrates a rather high degree of repeatability (i.e., precision) of our measurements of the illusion. Calculations of the grand-mean curve based on the individual data of the entire

group of observers (Fig. 6h; closed circles) showed that SEM values do not exceed 0.56 arcmin.

We assume that the specific behavior of the illusion found in the first series of Experiment 2 (vertically oriented arcs) can be explained by the manifestation of some additional effects that were not taken into account in our preliminary simplified theoretical reasoning (as mentioned earlier in the section of theoretical predictions). We hypothesize that these effects, again, may be associated with early two-dimensional spatial frequency filtering of abrupt changes in luminance at stimulus endpoints, which are absent in the case of full circles, but appear as a significant factor for circular arcs. To test the suggestion, we performed Experiment 3 with three-dot stimuli containing only the endpoints of imaginary arcs (Fig. 2e).

Experiment 3: Illusion caused by endpoints of imaginary circular arcs

As in Experiment 2, the radius of imaginary arcs was fixed at 25 arcmin, and their central angle randomly changed in a range from 0° to 180°.

As can be seen from the graphs in Fig. 6a-g (triangles), for most subjects, rather simple experimental curves were obtained: the magnitude of length misjudgments gradually decreases with the increase of the arc angle. The resulting pattern is easier to see for the grand-mean curve calculated for the entire group of observers (Fig. 6h; triangles); the values of SEM for the grand means do not exceed 0.69 arcmin. In accordance with our expectations regarding the essential role of the endpoints of the arcs in the illusion appearance, the values of the illusion magnitude obtained for small acute angles (in the range from 6° to 30°) are quite comparable with corresponding data (i.e., illusion magnitudes for short vertical arcs) collected in the first series of Experiment 2 (the paired *t*-test, *df* = 4, $\alpha = 0.05$: $t = 0.145$ [$P = 0.892$] with the preliminary Shapiro-Wilk test for the normality of residuals: $W = 0.913$ [$P = 0.487$]), and this fact also provides an additional argument in favor of a rather good precision of our experimental measurements. We think that, as in previous experiments, the effects related to an observer-specific way of stimuli viewing (e.g., different patterns of gaze fixation) may be responsible for some variability in the shape of the experimental curves (particularly in the case of subject S7, Fig. 6g, whose data indicate a near-zero slope of the curve for central angle values ranging from 0° to about 90°).

Comparison of experimental data with theoretical predictions

As follows from the experimental results obtained, stimuli with a distracting circle (outlined or uniformly filled) cause rather significant length-matching errors, which mainly confirms our preliminary guesses. With the aim of more thoroughly verifying the theoretical predictions, we approximated experimental data with the functions of our quantitative model based on the idea of local integration of distractor-evoked effects in the immediate vicinity of the terminators of stimulus spatial intervals (Bulatov et al., 2020). In all data approximations, the method of least squares with the implementation of sequential quadratic programming algorithm (LeastSquaresFit function, Mathcad, Parametric Technology Corporation) was used. To reduce the manifestation of irrelevant observer-specific factors, and to emphasize the most common regularities in the body of data gathered in the study, the grand means calculated for the entire group of observers were used in fitting the model parameters.

In order to approximate the data collected in experiments with full outlined circles (Fig. 5h; open circles), we used the following function that has three free parameters (*b*, *k*, and σ):

$$I_{out}(r, b, k, \sigma) = b + C_{out}(r, \sigma, k) \tag{5}$$

where *r* is the circle radius, *b* refers to a constant shift along the ordinate axis, *k* is a coefficient of proportionality, and $C_{out}(r, \sigma, k)$ represents the illusion magnitude caused by a full outlined circle in formula 2; σ refers to the standard deviation of the Gaussian profile of relevant AWS centered at the lateral stimulus terminator. The same set of free parameters was used in the model function to fit the data obtained in experiments with uniformly filled distractors (Fig. 5h; closed circles):

$$I_{fd}(r, b, k, \sigma) = b + C_{fd}(r, \sigma, k) \tag{6}$$

where $C_{fd}(r, \sigma, k)$ represents function 4.

The fitting of grand-mean curves demonstrated a good correspondence between the computational and experimental results (Fig. 7a,b; solid curves); the values of the coefficient of determination R^2 in all the cases were higher than 0.98 (Table 1).

Given the model’s assumptions, the magnitude of the illusion caused by the endpoints of imaginary circular arcs (Fig. 2e) can be evaluated as follows:

$$P_{end}(r, \phi, \sigma, k) \approx \int_{-\infty}^{\infty} \int_{\frac{\phi}{2}}^{\infty} W'(x, y, \sigma) \left(D'_{end}(x, y, \sigma, r) - T(x, y, \sigma) \right) dx dy = \frac{k}{\sigma^2} \int_{-\infty}^{\infty} \left(\int_{\frac{\phi}{2}}^{\infty} \left(x \cos\left(\frac{\phi}{2}\right) - y \sin\left(\frac{\phi}{2}\right) \right) e^{-\frac{x^2+y^2}{2\sigma^2}} \left(e^{-\frac{(x-r)^2+y^2}{2\sigma^2}} - e^{-\frac{x^2+y^2}{2\sigma^2}} \right) dx \right) dy = \frac{k}{4} \pi r \cos\left(\frac{\phi}{2}\right) e^{-\frac{r^2}{4\sigma^2}} \tag{7}$$

Table 1 The resulting parameters of fitting functions 5, 6, 8, 10, and 11 to relevant experimental data

Parameters	Distractor type				
	Outlined circle (Fig. 2a)	Filled circle (Fig. 2b)	Vertical arcs (Fig. 2c)	Horizontal arcs (Fig. 2d)	Arcs' endpoints (Fig. 2e)
b	-0.291±0.547	0.687±0.635	-0.074±1.471	0.718±1.343	1.942±0.843
k	1.229±0.079	2.246±0.228	1.3±0.15	1.306±0.142	1.113±0.115
σ	17.65±0.48	6.225±0.4	17.09	17.09	16.516±0.011
R^2	0.983	0.988	0.928	0.932	0.936
W, P_w	0.969, 0.488	0.971, 0.542	0.951, 0.166	0.951, 0.164	0.971, 0.598 ^a

b (%), constant component; k , coefficient of proportionality; σ (arcmin), the standard deviation of the Gaussian function; R^2 , coefficient of determination; W and P_w , the Shapiro-Wilk test statistic and p -value, respectively

^a first two data-points in Fig. 7c were excluded from statistical analysis

where r and ϕ represent the radius and the central angle of the arc, respectively; $W'(x,y,\sigma)$ represents the two-dimensional profile of the AWS rotated by $\frac{\pi}{2} - \phi/2$; $D'_{end}(x,y,\sigma,r) = e^{-\frac{(x-r)^2 + y^2}{2\sigma^2}}$, and $T(x,y,\sigma) = e^{-\frac{y^2 + \pi^2}{2\sigma^2}}$ represent the normalized two-dimensional profiles of neural excitation evoked by the distracting endpoint (tangentially displaced by $-\phi/2$) and the terminator-dot, respectively. Accordingly, the grand-mean curve (Fig. 6h; triangles) representing the data collected in experiments with the endpoints of imaginary distracting arcs was fitted by the function (with three free parameters b , k , and σ):

$$I_{end}(\phi, b, k, \sigma) = b + P_{end}(r, \phi, \sigma, k) \quad (8)$$

where $r = 25$ arcmin. As can be seen from the graph in Fig. 7c (solid curve), the approximation showed a fairly good agreement ($R^2 > 0.93$) between the calculated and experimental results (with some exceptions for very small values of the central angle, i.e., when the two endpoints of the arc practically merge into one).

As was noted above, the results of experiments with arcs oriented orthogonally to the stimulus axis (Fig. 2c) differ significantly from our simplified preliminary predictions. Therefore, we assumed that an influence of additional effects caused by the arcs' endpoints should be introduced in the model's calculations. Since the direct analytical estimation of the effects is rather difficult (due to the complex shape of the considered modified excitation profiles), it seems reasonable to suppose that the cumulative neural excitation evoked by the endpoint is proportional to some effective area $\eta_{dot}(\sigma) = \pi\sigma^2$ (where σ is the standard deviation of Gaussian profile of the relevant AWS) occupied by the corresponding two-dimensional profile. Likewise, the effective area associated with the excitation caused by the half-arc can be estimated as $\eta_{arc}(\phi, r, \sigma) = \phi r \sigma$ (where r and ϕ represent the radius and the central angle of the arc, respectively). Then, since the supposed endpoint-effects are most pronounced for very short arcs ($\phi \approx 0$) and vanish in the case of a full outlined circle ($\phi =$

π), the endpoint influence function can be defined as the ratio between the area $\eta_{dot}(\sigma)$ and the aggregated area $\eta_{dot}(\sigma) + \eta_{arc}(\phi, r, \sigma)$:

$$\begin{aligned} g(\phi, r, \sigma) &= \frac{\eta_{dot}(\sigma)(1 + \lambda)}{\eta_{dot}(\sigma) + \eta_{arc}(\phi, r, \sigma)} - \lambda \\ &= \frac{1 + \frac{\eta_{dot}(\sigma)}{\eta_{arc}(\pi, r, \sigma)}}{1 + \frac{\eta_{arc}(\phi, r, \sigma)}{\eta_{dot}(\sigma)}} - \frac{\eta_{dot}(\sigma)}{\eta_{arc}(\pi, r, \sigma)} \\ &= \frac{1 + \frac{\sigma}{r}}{1 + \frac{\phi r}{\pi \sigma}} - \frac{\sigma}{r} \end{aligned} \quad (9)$$

where λ is needed for the function normalization, i.e., $g(0, r, \sigma) = 1$ when the arc is absent, and $g(\pi, r, \sigma) = 0$ for the full circle.

Accordingly, in order to approximate the data (Fig. 6h; open circles) collected in experiments with vertically oriented circular arcs, we used the following function with only two free parameters (b and k):

$$I_{ver}(\phi, b, k) = \begin{cases} b, \phi = 0 \\ b + A_{ver}(r, \phi, \sigma_{arc}, k) + g(\phi, r, \sigma_{arc})P_{end}(r, \phi, \sigma_{arc}, k), 0 < \phi \leq \pi \end{cases} \quad (10)$$

where $A_{ver}(r, \phi, \sigma, k)$ and $P_{end}(r, \phi, \sigma, k)$ represent functions 2 and 7, respectively; $g(\phi, r, \sigma)$ is the endpoint influence function (formula 9); $r = 25$ arcmin represents the arc radius. With the aim of reducing the number of free parameters, we considered it expedient to use the arithmetic mean in the calculations, $\sigma_{arc} = (17.65 + 16.52)/2 = 17.09$ arcmin, of the corresponding values (Table 1) previously established in fittings (formulas 5 and 8) of the data from experiments with full outlined circles and with the endpoints of imaginary arcs. The same set of free parameters was used to fit the data (Fig. 6h; closed circles) obtained in experiments with horizontally oriented arcs:

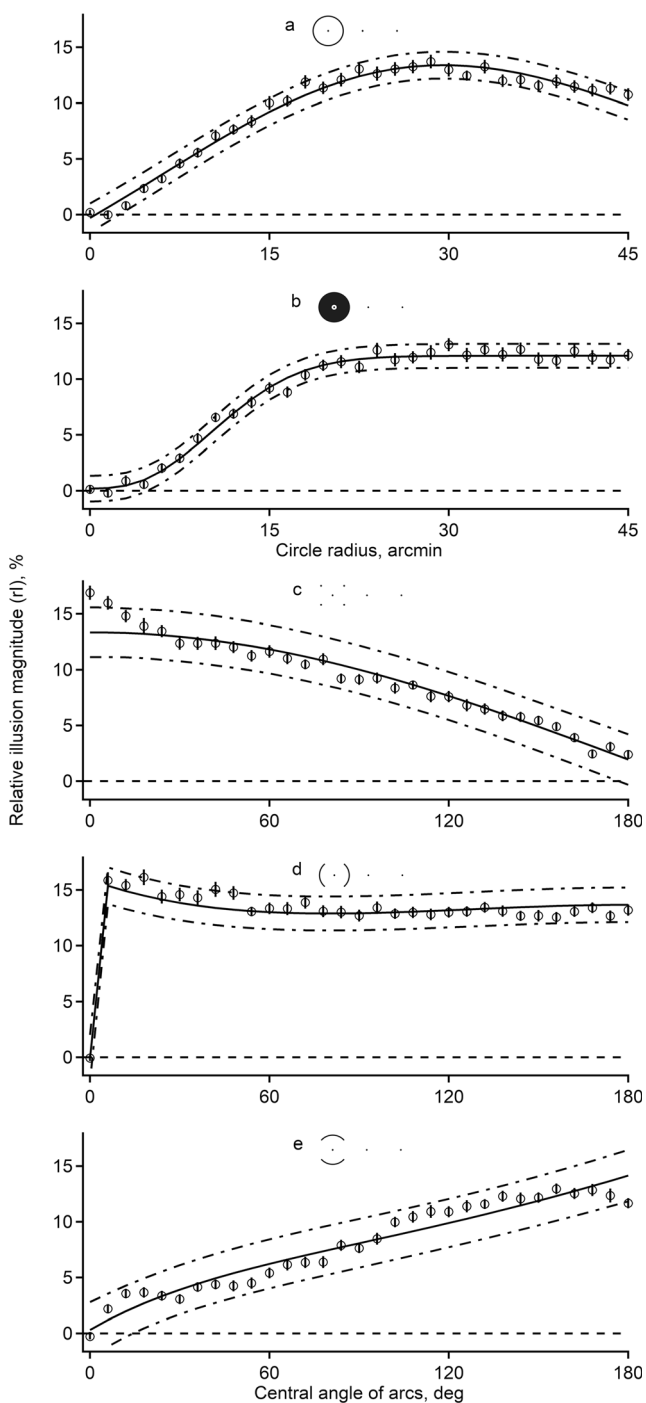


Fig. 7 The results of approximation of the grand-means data according to the model functions. In the graphs, open symbols represent the grand-mean data for stimuli with the outlined circle (a), the uniformly filled circle (b), the endpoints of the imaginary arcs (c), the vertical arcs (d), and the horizontal arcs (e), respectively. Solid curves represent the least squares fitting of the functions 5, 6, 8, 10, and 11 to relevant experimental data; dash-dot curves represent confidence intervals of the fitting. Error bars depict ± 1 standard error of the mean (SEM)

$$I_{hor}(\phi, b, k) = \begin{cases} b, & \phi = 0 \\ b + A_{hor}(r, \phi, \sigma_{arc}, k) + g(\phi, r, \sigma_{arc})G_{end}(r, \phi, \sigma_{arc}, k), & 0 < \phi \leq \pi \end{cases} \quad (11)$$

where $A_{hor}(r, \phi, \sigma, k)$ is function 3, and $G_{end}(r, \phi, \sigma, k)$ represents the modified (by substituting $\cos(\phi/2)$ with $\sin(\phi/2)$) function 7.

As can be seen from the graphs in Fig. 7d, e (solid curves), the approximations showed a good agreement between the calculated and experimental results; the values of the coefficient of determination R^2 were higher than 0.92 (Table 1).

With the aim of a more thorough examination of the goodness-of-fit, statistical analysis of all the data with the Shapiro-Wilk test (assessment of normality of residuals) was performed (Table 1). For each calculated curve, a matrix of partial derivatives of the model’s relevant function was multiplied by the residual mean square. These data allowed an additional evaluation of the goodness-of-fit by calculating confidence intervals for predicted values at each point along the range of the independent variable (Fig. 7; dash-dot curves).

Discussion

A sequential exploration of the principles underlying the recently proposed explanation (Bulatov et al., 2017; Bulatov et al., 2019) of the FSI made it possible to hypothesize the appearance of illusory effects caused by previously unknown modifications of stimuli. The aim of the present study was to check these predictions and verify whether the quantitative model of the FSI (Bulatov et al., 2020; Marma et al., 2020) is powerful enough to account for experimental data gathered with stimuli comprising distracting circles (either outlined or uniformly filled). The collected data demonstrate that the illusion does indeed arise and that the theoretical calculations performed adequately fit the changes of the illusion magnitude for various modifications of contextual distractors (Fig. 7, solid curves; Table 1). Therefore, it seems reasonable to conclude that the results obtained, at least to a first approximation, are consistent with the illusion’s explanation based on the idea of the perceptual displacement of stimulus terminators, caused, in turn, by a context-mediated increase in neural activity.

However, it should be noted that without additional assumptions, the proposed simplified quantitative model does not completely follow some of the relationships observed in experiments. The most important of the assumptions made is related to the manifestation of the processes of two-dimensional spatial frequency filtering. We supposed that because of this difference-of-Gaussians filtering, which is an inherent feature in even the lowest levels of the visual system (e.g., at the level of the retinal ganglion cells that have relatively small center-surround receptive fields), regions in the neural excitation profile corresponding to abrupt changes in stimulus luminance (e.g., surface boundaries or line ends) become significantly enhanced (Cao et al., 2019; Fang et al., 2020; Wei et al., 2013); later, this filtered information is

utilized by various higher-level visual mechanisms, some of which may be responsible for the filled-space (and related) illusion appearance. Since the putative two-dimensional profile of the AWS is anisotropic (i.e., not circularly symmetric, Fig. 3) with higher weights along the main (in our case, horizontal) stimulus axis, the manifestation of the corresponding filtering-induced distortions in the profile of neural excitation (and hence the deviation from predictions of the simplified model) should be mainly expressed for stimuli with short vertical distracting arcs, but should be significantly less for horizontal arcs (which is actually seen in the experimental data). Unfortunately, a direct analytical implementation of the filtering procedure in the model equations is currently not amenable due to significant computational difficulties (which can be considered as one of the interesting challenges for future research), so we used some simple empirically built function of the influence of endpoints (formula 9).

We believe that the absence of a significant difference between the experimental results for stimuli containing either uniformly filled or outlined distracting circles (Fig. 5h, closed and open symbols) can be considered as an additional argument in support of the suggestion concerning the manifestation of the effects of early spatial frequency filtering. Although the approximation (by function 6) of the grand-mean curve corresponding to the stimulus with the filled distractor demonstrated a rather good agreement between the computational and experimental data (Fig. 7b; solid curve), the resulting fitting parameters (Table 1) differ substantially from those obtained for outlined circles (i.e., much larger k : 2.246 ± 0.228 vs. 1.229 ± 0.079 , and a lot smaller σ : 6.225 ± 0.4 arcmin vs. 17.65 ± 0.48 arcmin). One of the straightforward ways to explain this discrepancy between the parameters could be the use of an oversimplification in formula 4 (i.e., approximation of the excitation profile by a piecewise-constant function), as well as the assumption that all subjects were necessarily inclined to direct their gaze closer to the lateral stimulus terminator (thereby using a smaller AWS during length-judgements). Of note, however, the numerical examinations of the model function 4 have shown that such a replacement by a piecewise-constant function has only a slight effect on the resulting calculations, while some specific modification of the excitation profile according to the appropriate spatial differentiation procedure (thus making $C_{fd}(r, \sigma, k)$ in function 6 more similar to $C_{out}(r, \sigma, k)$ in function 5, which is related to outlined distractors) offers much more consistent parameter values (and, e.g., direct fitting of the experimental data with function 5 gives $k = 1.265 \pm 0.113$ and $\sigma = 17.497 \pm 1.056$ arcmin). Therefore, in order to explain why the results of experiments with uniformly filled shapes do not differ from those obtained with the outlined ones, we consider it more reasonable to assume the manifestation of bandpass two-dimensional spatial frequency filtering (which inherently corresponds to the procedure of spatial differentiation that

increases the similarity of the excitation profiles evoked by objects sharing the same contour-shape). Moreover, this assumption is consistent with the results of numerous studies on perceptual positions, locating the centers of either outlined or uniformly filled stimuli (both moving and stationary), which demonstrated that the perceived position of the centers is determined solely by the configuration of the stimulus boundaries (Anstis et al., 2009; Baud-Bovy & Soechting, 2001; Bulatov et al., 2015; Proffitt et al., 1983; Proffitt & Cutting, 1980; Vos et al., 1993). Of note, we are fully aware that the above alternative explanation (by the spatial-frequency filtering) for resemblance of the experimental results obtained for the outlined and uniformly filled circles seems to be relatively weakly substantiated. Unfortunately, more strict argumentation is currently unavailable (due to significant difficulties in modifying model equations, as well as performing additional relevant experiments), which can be considered as one of the shortcomings of the present study, and which should be resolved in future research.

Besides the above-mentioned additional assumptions, the model uses several significant simplifications, and one of the most important issues is related to the procedure for normalization (or scaling) neural activity. According to numerous literature data (Carandini & Heeger, 2012; Olsen et al., 2010; Reynolds & Heeger, 2009; Vokoun et al., 2014), the normalization is a very common inherent feature of neural processing that provides invariant (with respect to various parameters) neural representation of stimuli. Ordinarily this procedure is reported in terms of the so-called divisive normalization (the neuronal response is divided by the integrated activity of neighboring neurons in the population). The direct analytical implementation of the divisive normalization leads to a significant complication of the derived formulas; therefore, in the current model calculations, a simple scaling of the excitation amplitude from 0 to 1 was applied, followed by the choice of the appropriate integration limits. As a result, such a simplification can cause certain inaccuracies (although not very large, judging by relevant numerical examinations) in the calculations of illusion parameters, especially in cases of close spatial proximity of different parts of the stimulus, when the corresponding excitation profiles overlap significantly (e.g., the ends of very short arcs).

As an example of other related factors not accounted for in the present modeling, higher-order complex processes of perceptual grouping (providing the size constancy and figural segregation) can be mentioned, which are likely to influence length judgments and, thus, can be associated with the illusion emergence (Noguchi et al., 1990; Tannazzo et al., 2014). However, it should be noted that most "higher-order processing" explanations tend to make only qualitative predictions, characterized by numerous and vague assumptions, most of which themselves need confirmation; therefore, their analytical formalization is rather difficult. On the contrary, the

present approach is based on a relatively small set of reasonably substantiated suggestions and is capable of making certain quantitative predictions that can be directly verified in experiments. In this regard, we believe that one of the key findings of the present study is that the proposed model is able to predict not only general trends in the behavior of the illusion, but also reveals some quantitative details, for example, by indicating specific shapes of the curves of functional dependences, which is clearly not typical for most of the currently known explanations of geometric illusions.

Unfortunately, there are currently no other quantitatively sufficiently developed theoretical studies of the FSI and related illusions (at least as far as we know); therefore, a direct comparison of the presented model with other relevant explanations is rather difficult. At the same time, it is necessary to assume that the proposed model adequately reproduces one of the most widely known features of the Opper-Kundt illusion – a non-monotonic dependence on the number of discrete fillers, established in numerous previous studies (Bulatov et al., 1997; Coren et al., 1976; Noguchi et al., 1990; Obonai, 1933; Piaget & Osterrieth, 1953; Spiegel, 1937; Wackermann & Kastner, 2010). The base principles underlying the model calculations are also consistent with experimental evidence regarding the illusion dependence on the gaze-fixation pattern when observing stimuli (Piaget & Bang, 1961). However, it should be emphasized that, due to its extreme simplicity, the proposed explanation does not pretend to identify any specific neural mechanisms (and even more so their localization in the brain) underlying the illusion origin, but rather suggests (by checking the reliability of predictions) trends for further research. It is obvious that a future successful theory should satisfactorily account for the effects arising from the perception of the widest possible range of stimulus modifications (including previously unknown ones); in this respect, we think that it is the computational quantitative interpretation of the phenomenon that is the approach that can offer a satisfactory unambiguous assessment of the illusion behavior for different variations of stimulus parameters.

According to the basic assumption of the FSI model, the magnitude of the illusion is highly dependent on the size of the corresponding AWS (which increases linearly with retinal eccentricity) and, therefore, should vary with the direction of the observer's stare. However, the lack of direct experimental data on the actual pattern of gaze fixations is one of the important flaws of the present study, which needs to be addressed in future investigations. Other critical assumptions used are related to manifestation of the processes of spatial frequency filtering and normalization of neural activity. In this regard, for a better understanding of the neural mechanisms underlying the illusion occurrence, further research is also needed to verify whether the proposed computational approach can be used in the explanation of the results of experiments with a more complicated distribution of filled stimulus luminance.

Conclusions

The aim of the present study was to verify the predictions of the computational model of the FSI regarding the manifestation of illusory effects caused by earlier untested stimuli that contain a distracting circle (either outlined or uniformly filled) surrounding one of the lateral terminators. It was shown in psychophysical experiments that the illusion magnitude changes predictably with the size of the circle and that there is no significant difference between the data obtained for stimuli with the outlined and filled distractors. However, it was also demonstrated that for a correct approximation of the relationships obtained in additional experiments with stimuli containing distracting circular arcs, it is necessary to make an extra assumption related to the manifestation of effects caused by two-dimensional spatial frequency filtering. To test the assumption, a supplementary experiment was carried out with stimuli containing only the ends of imaginary arcs. A sufficiently successful theoretical interpretation of the experimental results supports the hypothesis that perceptual positional displacements caused by additional context-induced neural excitation can be considered as one of the main causes of the filled-space illusion.

References

- Anstis, S., Gregory, R., & Heard, P. (2009). The triangle-bisection illusion. *Perception*, 38(3), 321–32.
- Bailes, S. M. (1995). *Effects of processing time and stimulus density on apparent width of the Opper-Kundt illusion* [Ph.D. Thesis]. Concordia University, Montréal, QC, CA.
- Baud-Bovy, G., & Soechting, J. (2001). Visual localization of the center of mass of compact, asymmetric, two-dimensional shapes. *Journal of Experimental Psychology: Human Perception and Performance*, 27(3), 692–706.
- Bertulis, A., & Bulatov, A. (2001). Distortions of length perception in human vision. *Biomedicine*, 1, 3–23.
- Bertulis, A., Surkys, T., Bulatov, A., & Bielevičius, A. (2014). Temporal dynamics of the Opper-Kundt illusion compared to the Müller-Lyer illusion. *Acta Neurobiologiae Experimentalis*, 74, 443–455.
- Blakemore, C., Carpenter, R.H.S., & Georgeson, M.A. (1970). Lateral inhibition between orientation detectors in the human visual system. *Nature*, 228, 37–39.
- Bremmer, F., Kaminiarz, A., Klingenhoefer, S., & Churan, J. (2016). Decoding target distance and saccade amplitude from population activity in the macaque Lateral Intraparietal Area (LIP). *Frontiers in Integrative Neuroscience*, 10, 30. <https://doi.org/10.3389/fnint.2016.00030>.
- Bulatov, A., & Bertulis, A. (2005). Superimposition of illusory patterns with contrast variations. *Acta Neurobiologiae Experimentalis*, 65, 51–60.
- Bulatov, A., Bertulis, A., & Mickienė, L. (1997). Geometrical illusions: study and modelling. *Biological Cybernetics*, 77, 395–406.
- Bulatov, A., Bulatova, N., Loginovich, Y., & Surkys, T. (2015). Illusion of extent evoked by closed two-dimensional shapes. *Biological Cybernetics*, 109, 163–178.
- Bulatov, A., Bulatova, N., Surkys, T., & Mickienė, L. (2017). An effect of continuous contextual filling in the filled-space illusion. *Acta Neurobiologiae Experimentalis*, 77, 157–167.

- Bulatov, A., Mamma, V., & Bulatova, N. (2020). Two-dimensional profile of the region of distractors' influence on visual length judgments. *Attention, Perception, & Psychophysics*, 82, 2714–2727.
- Bulatov, A., Mamma, V., Bulatova, N., & Mickienė, L. (2019). The filled-space illusion induced by a single-dot distractor. *Acta Neurobiologiae Experimentalis*, 79, 39–52.
- Cao, Y.-J., Lin, C., Pan, Y.-J., & Zhao, H.-J. (2019). Application of the center-surround mechanism to contour detection. *Multimedia Tools and Applications*, 78, 25121–25141.
- Carandini, M., & Heeger, D. J. (2012). Normalization as a canonical neural computation. *Nature Reviews Neuroscience*, 13, 51–62.
- Coren, S., Girgus, J. S., Ehrlichman, H., & Hakistan, A. R. (1976). An empirical taxonomy of visual illusions. *Perception & Psychophysics*, 20, 129–147.
- Craven, B.J., & Watt, R.J. (1989). The use of fractal image statistics in the estimation of lateral spatial extent. *Spatial Vision*, 4, 223–239.
- Dekker, T.M., Schwarzkopf, D.S., de Haas, B., Nardini, M., & Sereno, M.I. (2019). Population receptive field tuning properties of visual cortex during childhood. *Developmental Cognitive Neuroscience*, 37, 1–9. <https://doi.org/10.1016/j.dcn.2019.01.001>
- Dumoulin, S. O., & Wandell, B. A. (2008). Population receptive field estimates in human visual cortex. *NeuroImage*, 39(2), 647–660.
- Dworkin, L., & Bross, M. (1998). Brightness contrast and exposure time effects on the Oppel-Kundt illusion. *Perception* (Suppl.), 27, 87.
- Fang, T., Fan, Y., & Wu, W. (2020). Salient contour detection on the basis of the mechanism of bilateral asymmetric receptive fields. *Signal, Image and Video Processing*, 14, 1461–1469. <https://doi.org/10.1007/s11760-020-01689-1>
- Ganz, L. (1966). Mechanism of the figural aftereffects. *Psychological Review*, 73, 128–150.
- Giora, E., & Gori, S. (2010). The perceptual expansion of a filled area depends on textural characteristics. *Vision Research*, 50, 2466–2475.
- Graf, A. B., & Andersen, R. A. (2014). Inferring eye position from populations of lateral intraparietal neurons. *Elife*, 3:e02813. <https://doi.org/10.7554/eLife.02813>.
- Krauzlis, R. J., Goffart, L., & Hafed, Z. M. (2017). Neuronal control of fixation and fixational eye movements. *Philosophical Transactions of the Royal Society B: Biological Sciences*, 372(1718), 20160205.
- Long, G. M., & Murtagh, M. P. (1984). Task and size effects in the Oppel-Kundt and irradiation illusions. *Journal of General Psychology*, 111, 229–240.
- Mamma, V., Bulatov, A., & Bulatova, N. (2020). Dependence of the filled-space illusion on the size and location of contextual distractors. *Acta Neurobiologiae Experimentalis*, 80, 139–159.
- Morgan, M. J., Hole, G. J., & Glennerster, A. (1990). Biases and sensitivities in geometrical illusions. *Vision Research*, 30, 1793–1810.
- Morgan, M. J., Melmoth, D., & Solomon, J. A. (2013). Linking hypotheses underlying Class A and Class B methods. *Visual Neuroscience*, 30, 197–206.
- Noguchi, K. (2003). The relationship between visual illusion and aesthetic preference – an attempt to unify experimental phenomenology and empirical aesthetics. *Axiomathes*, 13, 261–281.
- Noguchi, K., Hilz, R., & Rentshler, I. (1990). The effect of grouping of adjacent contours on the Oppel-Kundt illusion. *Japanese Journal of Psychonomic Science*, 8, 57–60.
- Obonai, T. (1933). Contributions to the study of psychophysical induction: III. Experiments on the illusions of filled space. *Japanese Journal of Psychology*, 8, 699–720.
- Olsen, S. R., Bhandawat, V., & Wilson, R.I. (2010). Divisive normalization in olfactory population codes. *Neuron*, 66, 287–299.
- Piaget, J., & Bang, V. (1961). L'évolution de l'illusion des espaces divisés (Oppel-Kundt) en présentation tachistoscopique. *Archives de Psychologie*, 38, 1–21.
- Piaget, J., & Osterrieth, P. A. (1953). Recherches sur le développement des perceptions: XVII. L'évolution de l'illusion d'Oppel-Kundt en fonction de l'âge. *Archives de Psychologie*, 34, 1–38.
- Proffitt, D.R., & Cutting, J.E. (1980). Perceiving the centroid of curvilinearly bounded rolling shapes. *Perception and Psychophysics*, 28, 484–487.
- Proffitt, D. R., Thomas, M.A., & O'Brien, R.G. (1983). The roles of contour and luminance distribution in determining perceived centers within shapes. *Perception and Psychophysics*, 33(1), 63–71.
- Reynolds, J. H., & Heeger, D. J. (2009). The normalization model of attention. *Neuron*, 61, 168–185.
- Sereno, A. B., & Lehky, S. R. (2011). Population coding of visual space: comparison of spatial representations in dorsal and ventral pathways. *Frontiers in Computational Neuroscience*, 4, 159. <https://doi.org/10.3389/fncom.2010.00159>
- Silva, M. F., Brascamp, J. W., Ferreira, S., Castelo-Branco, M., Dumoulin, S. O., & Harvey, B. M. (2018). Radial asymmetries in population receptive field size and cortical magnification factor in early visual cortex. *NeuroImage*, 167, 41–52.
- Spiegel, H. G. (1937) Ueber den Einfluss des Zwischenfeldes auf gesehene Abstände. *Psychologische Forschung*, 21, 327–383.
- Steenrod, S. C., Phillips, M.H., & Goldberg, M.E. (2013). The lateral intraparietal area codes the location of saccade targets and not the dimension of the saccades that will be made to acquire them. *Journal of Neurophysiology*, 109, 2596–2605. <https://doi.org/10.1152/jn.00349.2012>.
- Surkys, T. (2007). *Influence of colour and luminance contrast on perceptual distortions of stimulus geometry* [Ph.D. Thesis]. Kaunas University of Medicine, Kaunas, LT.
- Tannazzo, T., Kurylo, D.D., & Bukhari, F. (2014). Perceptual grouping across eccentricity. *Vision Research*, 103, 101–108.
- Taylor, M.M. (1962). Geometry of a visual illusion. *Journal of the Optical Society of America*, 52, 565–569.
- Vokoun, C. R., Huang, X., Jackson, M. B., & Basso, M. A. (2014). Response normalization in the superficial layers of the superior colliculus as a possible mechanism for saccadic averaging. *The Journal of Neuroscience*, 34(23), 7976–7987.
- Vos, P.G., Bocheva, N., Yakimoff, N., & Helsen, E. (1993). Perceived locations in two-dimensional patterns. *Vision Research*, 15, 2157–2169.
- Wackermann, J. (2012). Determinants of filled/empty optical illusion: Influence of luminance contrast and polarity. *Acta Neurobiologiae Experimentalis*, 72, 412–420.
- Wackermann, J. (2017). The Oppel-Kundt illusion. In A. Shapiro, & D. Todorović (Eds.), *Oxford compendium of visual illusion* (pp. 303–307). Oxford University Press.
- Wackermann, J., & Kastner, K. (2009). Paradoxical form of filled/empty optical illusion. *Acta Neurobiologiae Experimentalis*, 69, 560–563.
- Wackermann, J., & Kastner, K. (2010). Determinants of filled/empty optical illusion: search for the locus of maximal effect. *Acta Neurobiologiae Experimentalis*, 70, 423–434.
- Watt, R.J. (1990). The primal sketch in human vision. In A. Blake, & T. Troscianko (Eds.), *AI and the Eye* (pp. 147–180). Wiley and Sons.
- Wei, H., Lang, B., & Zuo, Q. (2013). Contour detection model with multi-scale integration based on non-classical receptive field. *Neurocomputing*, 103, 247–262.
- Welbourne, L. E., Morland, A. B., & Wade, A. R. (2018). Population receptive field (pRF) measurements of chromatic responses in human visual cortex using fMRI. *NeuroImage*, 167, 84–94.

Publisher's note Springer Nature remains neutral with regard to jurisdictional claims in published maps and institutional affiliations.